Isospin composition of fission barriers

K. Godbey,^{1,*} Christian Ross,^{2,†} and A.S. Umar^{2,‡}

¹Facility for Rare Isotope Beams, Michigan State University, East Lansing, Michigan 48824, USA ²Department of Physics and Astronomy, Vanderbilt University, Nashville, TN, 37235, USA (Dated: October 15, 2024)

We employ a microscopic method to study how isospin affect the fission potential of ²⁴⁰Pu. Our approach uses constrained Hartree-Fock theory (CHF) which allows us to separately investigate the isoscalar and isovector properties of the nuclear energy density functional (EDF). By analyzing the isoscalar and isovector components of the EDF along the fission path we can assess the isovector contribution to fission barriers. We study this effect for the fully adiabatic path to scission. The isovector component of the fission potential is found to increase in magnitude as the nucleus evolves towards scission, exemplifying the importance of stringent constraints on the isovector sector of the nuclear EDF for reliable predictions of fission properties.

Introduction. Fission occurs in various complex quantum systems, such as atomic nuclei and atomic clusters. A robust theoretical formulation of the fission process represents a significant challenge in the field of quantum many-body physics, primarily because of the difficulties in developing an effective and computationally feasible approach to model the transition from a unified system to the creation of separate fragments [1–4]. In the context of atomic nuclei, most of the evolution is believed to unfold over a relatively long time scale. This comparatively slow progression allows for the initial treatment of nuclear fission as an adiabatic process, where the system transitions along a potential energy landscape characterized by macroscopic variables like shape elongation and asymmetry.

Microscopic methods have been extensively applied in the analysis of fission pathways, as evidenced by recent studies in references[5-24]. Most microscopic approaches to calculate static adiabatic fission potentials rely on mean-field approaches with the effective interaction given by a nuclear energy density functional (EDF). The majority of EDFs are determined for ground state properties of nuclei with neutronproton asymmetries ranging from small to moderate values, leaving the isovector parts of the EDFs relatively underconstrained [25]. The isovector part of the EDF plays an important role in determining properties of atomic nuclei, particularly those with large neutron-proton asymmetry [26– 29]. In addition to influencing nuclear structure properties such as isovector giant dipole resonances and beta decay rates the isovector part also significantly effects the neutron skin thickness for heavy nuclei, which is important in constraining the symmetry energy and consequently impacting neutron stars and other astrophysical phenomena such as nucleosynthesis [30,31]. Particularly for neutron-rich nuclei, the isovector characteristics of the interaction will become increasingly significant. Recently, we have shown that the isovector part of the EDF plays an important role in the microscopic calculation of fusion barriers [32]. In the case of fusion, the isovector contribution is critical to the N/Z equilibration that occurs when the two nuclei begin to interact [33], which in turn modifies the fusion barrier. Here, we adopt the same formalism to study isovector contribution of the EDF to the adiabatic fission potential of ²⁴⁰Pu. Next we discuss the methods used to obtain the fission barriers as well as the isoscalar and isovector decomposition. This is followed by the discussion of our results.

Formalism. Within the Hartree-Fock (HF) theory, the antisymmetric many-body wavefunction is taken to be a Slater determinant. This many-body state is then used to construct the action using an effective nucleon-nucleon interaction. Variation of this action with respect to single-particle states

$$\delta S = \delta \int \langle \Phi | \hat{H} - \lambda (\hat{Q} - Q_0) | \Phi \rangle = 0, \tag{1}$$

subject to a constraint operator \hat{Q} with the Lagrange multiplier λ , results in the constrained Hartree-Fock (CHF) equations, which forces the system to acquire a particular value of $Q_0 = \langle \Phi_0 | \hat{Q} | \Phi_0 \rangle$, where the states Φ_0 are the solutions of Eq. (1) for a particular choice of Q_0 . The numerical solution of the CHF equations using the gradient iteration method is given in Refs. [34–36]. If we employ an effective interaction such as the Skyrme interaction, the total energy of the system can be represented as an volume integral of an EDF [37]

$$E = \langle \Phi | \hat{H} | \Phi \rangle = \int d^3 \mathbf{r} \mathcal{H}(\mathbf{r}) , \qquad (2)$$

with $\langle \Phi | \Phi \rangle = 1$. The Skyrme EDF may be decomposed into isoscalar and isovector parts [38] (in addition to the conventional kinetic and Coulomb terms) as:

$$\mathcal{H}(\mathbf{r}) = \frac{\hbar^2}{2m} \tau_0 + \mathcal{H}_0(\mathbf{r}) + \mathcal{H}_1(\mathbf{r}) + \mathcal{H}_C(\mathbf{r}) . \tag{3}$$

The isoscalar and isovector terms carry an isospin index (I = 0, 1) for the energy densities, respectively. The isoscalar energy density $(\mathcal{H}_0(\mathbf{r}))$ depends on the isoscalar particle density, whereas the isovector energy density $(\mathcal{H}_1(\mathbf{r}))$ depends on the isovector particle density, which can be defined through the density operator

$$\hat{\rho}_{\rm I}(\mathbf{r}) = \sum_{\lambda=1}^{A} \delta(\mathbf{r} - \mathbf{r}_{\lambda}) \hat{a}_{\rm I}(\lambda) , \qquad (4)$$

where

$$< q|\hat{a}_{\rm I}|q'> = \begin{cases} (-1)^{\rm I} \delta_{qq'}, \ q = {\rm proton} \\ \delta_{qq'}, \ q = {\rm neutron} \end{cases}$$
 (5)

^{*} godbey@frib.msu.edu

[†] christian.ross@vanderbilt.edu

[‡] umar@compsci.cas.vanderbilt.edu

allowing us to define

$$\rho_{\rm I}(\mathbf{r}) = \begin{cases} \rho_n(\mathbf{r}) + \rho_p(\mathbf{r}), & \text{I} = 0\\ \rho_n(\mathbf{r}) - \rho_p(\mathbf{r}), & \text{I} = 1 \end{cases}$$
 (6)

These definitions, of course, prescribe analogous expressions for other densities and currents. Using the above definition various moments are given by

$$(q_{L0})_{\rm I} = \int d^3r r^L Y_{L0}(\hat{\mathbf{r}}) \rho_{\rm I}(\mathbf{r}). \tag{7}$$

The local gauge and Galilean invariant form of the EDF is given by [38]

$$\mathcal{H}_{\mathbf{I}}(\mathbf{r}) = C_{\mathbf{I}}^{\rho} \rho_{\mathbf{I}}^{2} + C_{\mathbf{I}}^{s} \mathbf{s}_{\mathbf{I}}^{2} + C_{\mathbf{I}}^{\Delta \rho} \rho_{\mathbf{I}} \Delta \rho_{\mathbf{I}}
+ C_{\mathbf{I}}^{\Delta s} \mathbf{s}_{\mathbf{I}} \cdot \Delta \mathbf{s}_{\mathbf{I}} + C_{\mathbf{I}}^{\tau} (\rho_{\mathbf{I}} \tau_{\mathbf{I}} - \mathbf{j}_{\mathbf{I}}^{2})
+ C_{\mathbf{I}}^{T} \left(\mathbf{s}_{\mathbf{I}} \cdot \mathbf{T}_{\mathbf{I}} - \overrightarrow{J}_{\mathbf{I}}^{2} \right) + C_{\mathbf{I}}^{\nabla J} \left(\rho_{\mathbf{I}} \nabla \cdot \mathbf{J}_{\mathbf{I}} + \mathbf{s}_{\mathbf{I}} \cdot (\nabla \times \mathbf{j}_{\mathbf{I}}) \right).$$
(8)

The density dependence of the coupling constants has been restricted to the C_1^ρ and C_1^s terms only which stems from the most common choice of Skyrme EDF. These density dependent coefficients contribute to the coupling of isoscalar and isovector fields in the Hartree-Fock Hamiltonian [38]. In static CHF calculations for even-even nuclei the time-odd terms, \mathbf{s} and \mathbf{j} in Eq. (8), are zero due to time-reversal invariance. Similarly, most Skyrme parametrizations do not include the C_1^T term in the functional.

The decomposition of the Skyrme EDF into isoscalar and isovector components makes it feasible to study isospin dependence of nuclear properties microscopically, both for nuclear reactions [32,39,40] as well as for nuclear structure [38]. This is possible for any approach that employs the Skyrme EDF. Here, we implement the decomposed Skyrme EDF to study isospin effects in fission barriers coming from a constrained approach. Utilizing the decomposition of the Skyrme EDF [Eqs. (3 and 8)], we can re-write the energy along the constraint path as

$$E(Q_0) = \sum_{I=0} E_I(Q_0) , \qquad (9)$$

where $E_{\rm I}(Q_0)$ denotes the energy of the system computed by using the isoscalar and isovector parts of the Skyrme EDF given in Eqs. (3) and (8). The isoscalar energy term also includes the contributions from the kinetic energy and Coulomb terms. The Coulomb potential is solved from the typical three-dimensional Poisson equation (where the Slater approximation is used for the Coulomb exchange term) via Fast-Fourier Transform techniques. In practice it is more convenient to subtract the ground state energies to define the fission potential as

$$V_{I}(Q_{0}) = E_{I}(Q_{0}) - E_{I}^{g.s.}(Q_{0})$$

$$V(Q_{0}) = \sum_{I=0,1} V_{I}(Q_{0}).$$
(10)

Results. Applying the formalism detailed above, we now present the adiabatic fission potentials of ²⁴⁰Pu using the CHF

method. This nucleus is well-motivated as it has been shown that data on its fission isomer strongly impacts the resulting EDF calibration, particularly in the symmetry energy and its slope [41]. The Skyrme energy density functional SLy4d [42] was used with pairing treated at the BCS level. The pairing scheme was adopted to be the same as in the EV8 code [43], a density dependent surface pairing contact interaction with Fermi function cutoffs [43–45]. This was done to allow for comparison of the results calculated with the EV8 code.

The code used here was the VU-TDHF code which assumes no quantal or geometrical symmetries or approximations and includes the full Skyrme interaction, including the time-odd terms [46,47]. Unrestricted symmetry calculations of the fission potential is much more computationally intensive in comparison to axially symmetric or three-dimensional codes that impose planar symmetries. The VU-TDHF code uses basis-spline discretization and a gradient iteration method [48] for highly accurate calculations at a reasonable computational cost. The numerical implementation of the constrained iterations are described in Refs. [34,36]. While we do have possibility of imposing multiple constraints, we have only used the quadrupole constraint

$$q_{20} = \sqrt{\frac{5}{16\pi}} \int d^3r \rho(\mathbf{r})(2z^2 - x^2 - y^2),$$

in steps of $100 \text{ } fm^2$ starting from the ground state, with deformation 907 fm^2 , up to 12000 fm^2 (note that some studies do not include the factor $\sqrt{5/16\pi}$ in the definition of the quadrupole constraint). This allows the system to find the minimum energy configuration given the defined elongation of the nucleus. These configurations may involve arbitrary deformations, including triaxiality as discussed later. At the final constraint step the fragments are separated by R = 17.7 fm. The final light fragment average mass and charge is found to be A = 107.71 and Z = 43.28 with corresponding values for the heavy fragment being A = 132.29and Z = 50.72. These values are in agreement with those found in a recent study using the constrained Hartree-Fock Bogoliubov (CHFB) method [51]. The numerical box size was $50 \times 32 \times 32$ fm with mesh spacing of 1 fm. As an additional check we have also performed a backward constraint, starting from the final separated fragments, which coincided with the same curve.

In Fig. 1 we show the fission potentials for 240 Pu calculated with different codes and in one case a different EDF. Our results are depicted by the blue curve, while the fission potential calculated for the asymmetric fission using the EV2 code, a more general version of EV8 [43] that includes the possibility of parity breaking, is shown with the solid black curve [49]. The symmetric fission potential of EV8 is shown by the dashed black curve. For comparison we have also plotted the fission potential using the SeaLL1 EDF of Ref. [50] as the orange color curve. The fully unrestricted constraint procedure starts with an axially symmetric ground state with no octupole deformation and continues as such until about $4700 \ fm^2$. Beyond this point we move towards the symmetric fission channel. However, by tightening the constraint convergence criteria, and after many iterations, the system falls back

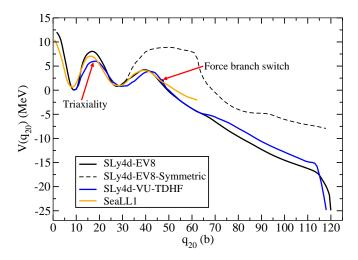


FIG. 1. Fission potentials for ²⁴⁰Pu calculated with different codes and functionals. Our results are depicted by the blue curve, while the EV8 results for asymmetric fission is shown with the solid black curve [49]. The symmetric fission potential of EV8 is shown by the dashed black curve. For comparison we have also plotted the fission potential using the SeaLL1 EDF of Ref. [50] as the orange color curve.

onto the asymmetric branch developing an octupole deformation. The lower first barrier height is due to the presence of triaxiality [52–54] that is explored in our calculations as compared to the results from the EV8 code, where the calculations where limited to axial symmetry for ease of use. We also observe that the switch to the symmetric fission branch occurs later in our case for the same reason.

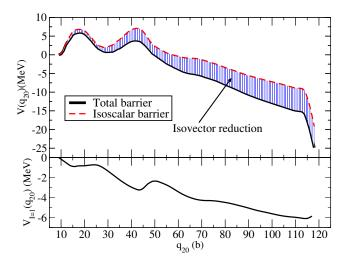


FIG. 2. Total (solid line) and isoscalar (dashed line) fission barriers for ²⁴⁰Pu is shown on the upper panel. The shaded region depicts the reduction of the fission barrier due to isovector contribution. The bottom panel shows the isovector potential as well as the potential corresponding to time-dependent scission case (dotted line).

In the upper panel of Fig. 2 we plot the total fission barrier as well as the one originating specifically from the isoscalar

part of the EDF. The shaded region shows the reduction of the total barrier due to isovector contribution. This reduction of the potential leads naturally to an enhancement in overall fission probabilities. The bottom panel of Fig. 2 shows the isovector contribution only. We observe that the isovector contribution acts to lower the isoscalar barrier throughout the fission potential

In Fig. 3 we plot the variation of the total and isovector octupole and hexadecupole moments as a function of the total quadrupole moment. As we see from the top panels the system starts with an axially symmetric configuration with no octupole deformation and in the vicinity of $q_{20} = 4500 \text{ fm}^2$ it makes a relatively rapid transition to acquire an octupole deformation. This is the case for both total and isovector octupole moments with isovector part having a lower strength. The transition to acquire an octupole deformation is somewhat dependent on the theoretical approach used to calculate the fission potential, with full HFB calculations yielding a smoother transition [51]. The hexadecupole moment has a smoother evolution through the transition point and again grows in a somewhat linear fashion with increasing quadrupole moment.

Over the years various experiments have been done to measure the height and depth of fission barriers for the ²⁴⁰Pu nucleus [55–60]. Bases on these the inner fission barrier height is predicted to be approximately 6.05 MeV, second minimum around 2.8 MeV, and outer fission barrier height to be around 5.15 MeV. In our calculations the isoscalar inner barrier height is 6.6 MeV, the first minimum depth is 2.2 MeV, and the outer barrier height is 6.0 MeV. The corresponding total potential values are; inner barrier height of 6.0 MeV, first minimum depth of 0.82 MeV, and outer barrier height of 3.9 MeV. From these values we see that the isovector contribution significantly reduces the the depth of the inner barrier to be much lower than the experimental value as well as a significant reduction in the height of the outer barrier. The very low inner barrier depth is a common problem in most studies using various EDFs.

Discussion. There is growing evidence that the isovector part of the nuclear energy density functionals play an important role for a multitude of structure and reaction properties. With the increasing availability of neutron and proton rich nuclei produced in radioactive ion-beam facilities more data should be available to better ascertain the contribution of the isovector components to the EDF. The isovector contributions do not only arise from the core EDF but also from the spinorbit [61,62] and pairing parts [63]. We have undertaken a study to discern the isoscalar and isovector contributions to the one-dimensional fission potential. The fission potential was calculated using a three-dimensional solver with no symmetry restrictions and the SLy4d EDF was used to facilitate comparison with other calculations. A natural future extension to this approach would be to extend the analysis to studies of potential energy surfaces and systems that exhibit multimodal fission, though this represents a substantial increase in computational effort.

We observe that the isovector part of the EDF makes a substantial contribution to the fission potential along the fis-

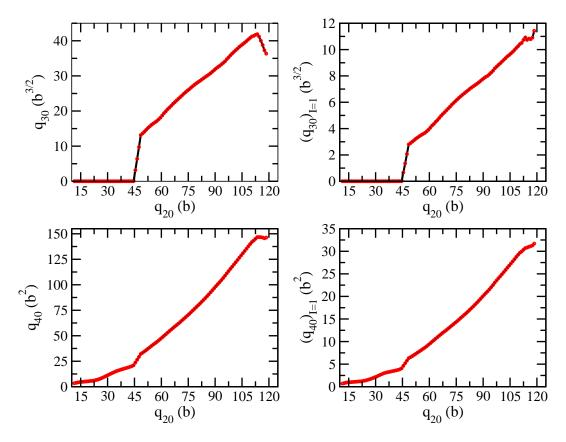


FIG. 3. The evolution of total and isovector octupole and hexadecupole moments as a function of the total quadrupole moment.

sion trajectory, accumulating influence as the system nears the scission point. This raises the question as to how well we constrain the isovector part of the EDF, including the isovector dependence of the spin-orbit interaction. That fusion and fission properties are important to constraining this sector is not new, though the consistent increase along the fission pathway implies that observables that are strongly impacted by the elongation of the system at scission are likely to contain more information than the first barrier and fission isomer alone. Naturally, any improvement to the isovector EDF would necessitate simultaneous consideration of the isoscalar part as well. Finally, a proper treatment of superfluidity, especially for the scission process that benefits from a dynamical pairing approach such as the time-dependent HFB, may introduce further improvements to pin down the isovector properties of the

EDF. During the dynamical scission and final phase of fragment formation, the rearrangement of nucleons due to shell effects influencing the N/Z equilibration will become very important in a way somewhat similar to the initial stages of the fusion process. Furthermore, some of the terms that vanish in the static calculations become relevant during the dynamics, meaning that observables sensitive to those dynamics (such as the total kinetic energy) are the only hope one has of providing a strong constraint.

ACKNOWLEDGMENTS

This work has been supported by the U.S. Department of Energy under award Nos. DE-SC0013847 (Vanderbilt University) and DE-NA0004074 (NNSA, the Stewardship Science Academic Alliances program).

N. Schunck and L. M. Robledo, Microscopic theory of nuclear fission: a review, Rep. Prog. Phys. 79, 116301 (2016).

^[2] A. N. Andreyev, K. Nishio, and K.-H. Schmidt, Nuclear fission: a review of experimental advances and phenomenology, Rep. Prog. Phys. 81, 016301 (2017).

^[3] M. Bender, R. Bernard, G. Bertsch, S. Chiba, J. J. Dobaczewski, N. Dubray, S. Giuliani, K. Hagino, D. Lacroix, Z. Li, P. Magierski, J. Maruhn, W. Nazarewicz, J. Pei, S. Péru-Desenfants, N. Pillet, J. Randrup, D. Regnier, P.-G. Reinhard, L. M. Robledo, W. Ryssens, J. Sadhukhan, G. Scamps, N. Schunck,

C. Simenel, J. Skalski, I. Stetcu, P. Stevenson, A. S. Umar, M. Verriere, D. Vretenar, M. Warda, and S. Åberg, Future of Nuclear Fission Theory, J. Phys. G: Nucl. Part. Phys. 47, 113002 (2020).

^[4] N. Schunck and D. Regnier, Theory of nuclear fission, Prog Part Nucl Phys 125, 103963 (2022).

^[5] N. Dubray, H. Goutte, and J.-P. Delaroche, Structure properties of ²²⁶Th and ^{256,258,260}Fm fission fragments: Mean-field analysis with the Gogny force, Phys. Rev. C 77, 014310 (2008).

^[6] H. Goutte, J. F. Berger, P. Casoli, and D. Gogny, Microscopic

- approach of fission dynamics applied to fragment kinetic energy and mass distributions in ²³⁸U, Phys. Rev. C **71**, 024316 (2005).
- [7] L. Bonneau, Fission modes of ²⁵⁶Fm and ²⁵⁸Fm in a microscopic approach, Phys. Rev. C **74**, 014301 (2006).
- [8] A. Staszczak, A. Baran, J. Dobaczewski, and W. Nazarewicz, Microscopic description of complex nuclear decay: Multimodal fission, Phys. Rev. C 80, 014309 (2009).
- [9] J. C. Pei, W. Nazarewicz, J. A. Sheikh, and A. K. Kerman, Fission Barriers of Compound Superheavy Nuclei, Phys. Rev. Lett. 102, 192501 (2009).
- [10] W. Younes and D. Gogny, Nuclear Scission and Quantum Localization, Phys. Rev. Lett. 107, 132501 (2011).
- [11] M. Warda and J. L. Egido, Fission half-lives of superheavy nuclei in a microscopic approach, Phys. Rev. C 86, 014322 (2012).
- [12] H. Abusara, A. V. Afanasjev, and P. Ring, Fission barriers in covariant density functional theory: Extrapolation to superheavy nuclei, Phys. Rev. C 85, 024314 (2012).
- [13] M. Mirea, Microscopic description of energy partition in fission fragments, Phys. Lett. B 717, 252 (2012).
- [14] B.-N. Lu, E.-G. Zhao, and S.-G. Zhou, Potential energy surfaces of actinide nuclei from a multidimensional constrained covariant density functional theory: Barrier heights and saddle point shapes, Phys. Rev. C 85, 011301 (2012).
- [15] A. Staszczak, A. Baran, and W. Nazarewicz, Spontaneous fission modes and lifetimes of superheavy elements in the nuclear density functional theory, Phys. Rev. C 87, 024320 (2013).
- [16] J. D. McDonnell, W. Nazarewicz, and J. A. Sheikh, Third minima in thorium and uranium isotopes in a self-consistent theory, Phys. Rev. C 87, 054327 (2013).
- [17] Jhilam Sadhukhan, K. Mazurek, A. Baran, J. Dobaczewski, W. Nazarewicz, and J. A. Sheikh, Spontaneous fission lifetimes from the minimization of self-consistent collective action, Phys. Rev. C 88, 064314 (2013).
- [18] N. Schunck, D. Duke, H. Carr, and A. Knoll, Description of induced nuclear fission with Skyrme energy functionals: Static potential energy surfaces and fission fragment properties, Phys. Rev. C 90, 054305 (2014).
- [19] M. Verriere and D. Regnier, The Time-Dependent Generator Coordinate Method in Nuclear Physics, Front. Phys. 8, 233 (2020)
- [20] R. Bernard, C. Simenel, and G. Blanchon, Quantum shell effects on the path to fission of atomic nuclei, Submitted (2021).
- [21] Bernard, R. N., Simenel, C., and Blanchon, G., Hartree-Fock-Bogoliubov study of quantum shell effects on the path to fission in ¹⁸⁰Hg, ²³⁶U and ²⁵⁶Fm, Eur. Phys. J. A **59**, 51 (2023).
- [22] E. Flynn, D. Lay, S. Agbemava, P. Giuliani, K. Godbey, W. Nazarewicz, and J. Sadhukhan, Nudged elastic band approach to nuclear fission pathways, Phys. Rev. C 105, 054302 (2022).
- [23] D. Lay, E. Flynn, S. Agbemava, K. Godbey, W. Nazarewicz, S. A. Giuliani, and J. Sadhukhan, Multimodal fission from selfconsistent calculations, Phys. Rev. C 109, 044306 (2024).
- [24] Y.-T. Qiu and J.-Y. Guo, Research on the static fission properties of ²⁴⁰Pu within the reflection asymmetric relativistic mean-field theory, Phys. Rev. C 109, 044301 (2024).
- [25] K. Godbey, A. S. Umar, and C. Simenel, Theoretical uncertainty quantification for heavy-ion fusion, Phys. Rev. C 106, L051602 (2022).
- [26] M. Bender, P.-H. Heenen, and P.-G. Reinhard, Self-consistent mean-field models for nuclear structure, Rev. Mod. Phys. 75, 121 (2003).
- [27] D. Vretenar, A. Afanasjev, G. Lalazissis, and P. Ring, Relativistic Hartree–Bogoliubov theory: static and dynamic aspects of exotic nuclear structure, Phys. Rep. 409, 101 (2005).

- [28] J. R. Stone and P.-G. Reinhard, The Skyrme interaction in finite nuclei and nuclear matter, Prog. Part. Nucl. Phys. 58, 587 (2007).
- [29] J. A. Sheikh, N. Hinohara, J. Dobaczewski, T. Nakatsukasa, W. Nazarewicz, and K. Sato, Isospin-invariant Skyrme energydensity-functional approach with axial symmetry, Phys. Rev. C 89, 054317 (2014).
- [30] B.-A. Li, L.-W. Chen, and C. M. Ko, Recent progress and new challenges in isospin physics with heavy-ion reactions, Phys. Rep. 464, 113 (2008).
- [31] M. Baldo and G. F. Burgio, The nuclear symmetry energy, Prog. Part. Nucl. Phys. 91, 203 (2016).
- [32] K. Godbey, A. S. Umar, and C. Simenel, Dependence of fusion on isospin dynamics, Phys. Rev. C 95, 011601(R) (2017).
- [33] C. Simenel, K. Godbey, and A. S. Umar, Timescales of Quantum Equilibration, Dissipation and Fluctuation in Nuclear Collisions, Phys. Rev. Lett. 124, 212504 (2020).
- [34] A. S. Umar, M. R. Strayer, R. Y. Cusson, P.-G. Reinhard, and D. A. Bromley, Time-dependent Hartree-Fock calculations of ${}^{4}\text{He} + {}^{14}\text{C}$, ${}^{12}\text{C} + {}^{12}\text{C}(0^+)$, and ${}^{4}\text{He} + {}^{20}\text{Ne}$ molecular formations, Phys. Rev. C **32**, 172 (1985).
- [35] R. Y. Cusson, P.-G. Reinhard, M. R. Strayer, J. A. Maruhn, and W. Greiner, Density as a constraint and the separation of internal excitation energy in TDHF, Z. Phys. A 320, 475 (1985).
- [36] A. S. Umar and V. E. Oberacker, Microscopic calculation of heavy-ion potentials based on TDHF, J. Phys. Conf. Ser. 402, 012038 (2012).
- [37] Y. M. Engel, D. M. Brink, K. Goeke, S. J. Krieger, and D. Vautherin, Time-dependent Hartree-Fock theory with Skyrme's interaction, Nucl. Phys. A 249, 215 (1975).
- [38] J. Dobaczewski and J. Dudek, Time-odd components in the mean field of rotating superdeformed nuclei, Phys. Rev. C 52, 1827 (1995).
- [39] K. Vo-Phuoc, C. Simenel, and E. C. Simpson, Dynamical effects in fusion with exotic nuclei, Phys. Rev. C 94, 024612 (2016).
- [40] R. Gumbel, C. Ross, and A. S. Umar, Role of isospin composition in low-energy nuclear fusion, Phys. Rev. C 108, L051602 (2023).
- [41] M. Kortelainen, J. McDonnell, W. Nazarewicz, P.-G. Reinhard, J. Sarich, N. Schunck, M. V. Stoitsov, and S. M. Wild, Nuclear energy density optimization: Large deformations, Phys. Rev. C 85, 024304 (2012).
- [42] Ka-Hae Kim, Takaharu Otsuka, and Paul Bonche, Threedimensional TDHF calculations for reactions of unstable nuclei, J. Phys. G: Nucl. Part. Phys. 23, 1267 (1997).
- [43] W. Ryssens, V. Hellemans, M. Bender, and P.-H. Heenen, Solution of the Skyrme–HF+BCS equation on a 3D mesh, II: A new version of the Ev8 code, Comput. Phys. Commun. 187, 175 (2015).
- [44] M. Bender, K. Rutz, P.-G. Reinhard, and J. A. Maruhn, Pairing gaps from nuclear mean-field models, Eur. Phys. J. A 8, 59
- [45] J. Dobaczewski, W. Nazarewicz, and T. R. Werner, Closed shells at drip-line nuclei, Phys. Scr. T56, 15 (1995).
- [46] A. S. Umar, M. R. Strayer, J. S. Wu, D. J. Dean, and M. C. Güçlü, Nuclear Hartree-Fock calculations with splines, Phys. Rev. C 44, 2512 (1991).
- [47] A. S. Umar and V. E. Oberacker, Three-dimensional unrestricted time-dependent Hartree-Fock fusion calculations using the full Skyrme interaction, Phys. Rev. C 73, 054607 (2006).
- [48] C. Bottcher, M. R. Strayer, A. S. Umar, and P.-G. Reinhard, Damped relaxation techniques to calculate relativistic boundstates, Phys. Rev. A 40, 4182 (1989).

- [49] Guillaume Scamps, Private Communication (2024).
- [50] Aurel Bulgac, Michael McNeil Forbes, Shi Jin, Rodrigo Navarro Perez, and Nicolas Schunck, Minimal nuclear energy density functional, Phys. Rev. C 97, 044313 (2018).
- [51] L. Tong and S. Yan, Microscopic investigations into fission dynamics beyond the saddle point, Phys. Rev. C 106, 044611 (2022).
- [52] H. Abusara, A. V. Afanasjev, and P. Ring, Fission barriers in actinides in covariant density functional theory: The role of triaxiality, Phys. Rev. C 82, 044303 (2010).
- [53] J. Sadhukhan, J. Dobaczewski, W. Nazarewicz, J. A. Sheikh, and A. Baran, Pairing-induced speedup of nuclear spontaneous fission, Phys. Rev. C 90, 061304 (2014).
- [54] K. Benrabia, D. E. Medjadi, M. Imadalou, and P. Quentin, Triaxial quadrupole dynamics and the inner fission barrier of some heavy even-even nuclei, Phys. Rev. C 96, 034320 (2017).
- [55] H. J. Specht, Nuclear fission, Rev. Mod. Phys. 46, 773 (1974).
- [56] R. Vandenbosch, Spontaneously Fissioning Isomers, Annu. Rev. Nucl. Part. Sci. 27, 1 (1977).

- [57] V. Metag, D. Habs, and H. Specht, Spectroscopic properties of fission isomers, Phys. Rep. 65, 1 (1980).
- [58] S. Bjørnholm and J. E. Lynn, The double-humped fission barrier, Rev. Mod. Phys. 52, 725 (1980).
- [59] P. G. Thirolf and D. Habs, Spectroscopy in the second and third minimum of actinide nuclei, Prog. Part. Nucl. Phys. 49, 325 (2002).
- [60] B. Singh, R. Zywina, and R. B. Firestone, Table of Superdeformed Nuclear Bands and Fission Isomers: Third Edition, Nucl. Data Sheets 97, 241 (2002).
- [61] M. M. Sharma, G. Lalazissis, J. König, and P. Ring, Isospin Dependence of the Spin-Orbit Force and Effective Nuclear Potentials, Phys. Rev. Lett. 74, 3744 (1995).
- [62] T.-G. Yue, Z. Zhang, and L.-W. Chen, PREX and CREX: Evidence for Strong Isovector Spin-Orbit Interaction (2024), arXiv:2406.03844 [nucl-th].
- [63] M. Yamagami, J. Margueron, H. Sagawa, and K. Hagino, Isoscalar and isovector density dependence of the pairing functional determined from global fitting, Phys. Rev. C 86, 034333 (2012).